

The Simulation Method of the Galvanic Coupling Intrabody Communication With Different Signal Transmission Paths

Yong Song, Qun Hao, Kai Zhang, Ming Wang, Yifang Chu, and Bangzhi Kang

Abstract—The simulation method plays an important role in the investigation of the intrabody communication (IBC). Due to the problems of the transfer function and the corresponding parameters, only the simulation of the galvanic coupling IBC along the arm has been achieved at present. In this paper, a method for the mathematical simulation of the galvanic coupling IBC with different signal transmission paths has been introduced. First, a new transfer function of the galvanic coupling IBC was derived with the consideration of the internal resistances of the IBC devices. Second, the determination of the corresponding parameters used in the transfer function was discussed in detail. Finally, both the measurements and the simulations of the galvanic coupling IBC along the different signal transmission paths were carried out. Our investigation shows that the mathematical simulation results coincide with the measurement results over the frequency range from 100 kHz to 5 MHz, which indicates that the proposed method offers the significant advantages in the theoretical analysis and the application of the galvanic coupling IBC.

Index Terms—Galvanic coupling, intrabody communication (IBC), mathematical simulation, personal area network, transfer function.

I. INTRODUCTION

INTRABODY communication (IBC) is a technology using the human body as a transmission medium for electrical signals. IBC technology offers a novel data communication in many fields. For instance, both high transmission quality and high signal transmission speed can be achieved by using IBC in the personal area network [1], [2], network access can be achieved by the motions (touch, stand, sit down, etc.) of the human body with the IBC devices [2], the implant biomedical monitoring of the human body can be implemented by the data communication of the IBC [3], and compared with the short-distance wireless technologies, IBC technology is more energy saving [4]. Therefore, IBC is believed to be a novel and promising technology for the short-distance communication in the future.

Manuscript received June 9, 2010; revised September 8, 2010; accepted September 9, 2010. Date of publication November 15, 2010; date of current version March 8, 2011. This work was supported in part by the National Natural Science Foundation of China under Grant 60801050 and in part by the Basic Research Foundation of the Beijing Institute of Technology of China under Grant 1010050320804. The Associate Editor coordinating the review process for this paper was Dr. Kurt Barbe.

The authors are with the School of Optoelectronics, Beijing Institute of Technology, Beijing, 100081 China (e-mail: yongsong@bit.edu.cn).

Color versions of one or more of the figures in this paper are available online at <http://ieeexplore.ieee.org>.

Digital Object Identifier 10.1109/TIM.2010.2087870

In general, the IBC approach can be divided into two types, which include the electrostatic coupling type [2] and the galvanic coupling type [8], as shown in Fig. 1. In the electrostatic coupling IBC, a return path is formed by the electrical coupling between the transmitting electrodes and the receiving electrodes through the external ground, while the signal is transmitted between the transmitter and the receiver by making a current loop [9]. It should be noted that the transmission quality of this approach is influenced by the surrounding environment. Moreover, there is a strong relativity between the electrode sizes and the coupling current, which results in the big size of the electrodes. In the second type which is the galvanic coupling IBC, the electrical signals are considered as the electromagnetic waves [8], and the electromagnetic signal transmits from a pair of transmitting electrodes to a pair of receiving electrodes within the human body directly. As a result, the signal transmission quality is not influenced by the individual's surroundings [10]. Meanwhile, the miniaturized electrode can also be used in this approach. Therefore, the galvanic coupling IBC is presented as a promising approach for the data communication within the human body [3], [5].

To guarantee the safety of the human body, the software simulation is considered as an important method for the investigation of the IBC. Two methods have been used for the simulation of the IBC. One is the finite-element method [6], [7] in which the finite model of the human body is developed first; then, the IBC simulation can be implemented using the finite-element method. Due to the big size and the complexity of the human body, huge data will be generated when modeling the whole human body, and the simulation accuracy is not satisfactory. The other method can be called the transfer function method [4], [12] in which the transfer function based on the circuit model is derived to describe the mathematical relation among the signal transmission paths within the human body, transmitter, receiver, electrodes, etc. Thus, the IBC simulation can be achieved by using the developed transfer functions. Compared with the finite-element method, this method is easy to be implemented and generates few data. Therefore, the transfer function method is believed as an available method to realize the IBC simulation within the lower frequency range.

The galvanic coupling IBC will be used in the data communication among the devices attached on the human skin or the sensors implanted in the human tissue for building a network [1]–[3]. Hence, the simulation of the IBC with different signal transmission paths is very important for simulating the data

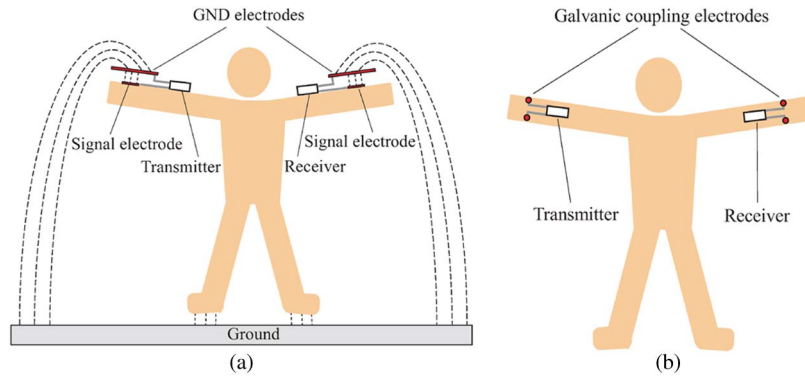


Fig. 1. Approaches for the IBC. (a) Electrostatic coupling type. (b) Galvanic coupling type.

transmission of the devices located in the different parts of the human body. Unfortunately, only the IBC simulation within the arm has been achieved at present [8], [12]. On the other hand, a simple four-terminal circuit model of the galvanic coupling IBC has been proposed. However, due to some important parameters, such as the coupling impedance between the electrodes and the human skin, the internal resistances of the IBC devices and the resistors of the human body, were not considered in the proposed transfer function [8], [12], a close agreement between the simulation results and the *in vivo* measurement results was not achieved. Meanwhile, the methods to determine the corresponding parameters used in the transfer function were not discussed in detail. Therefore, it is difficult to implement the simulation of the galvanic coupling IBC with different signal transmission paths by using these transfer functions.

In this paper, a method for the mathematical simulations of the galvanic coupling IBC with different signal transmission paths has been introduced. We first proposed a galvanic coupling IBC circuit model with the internal resistance of the IBC devices, while a new transfer function of the galvanic coupling IBC was derived. Second, we discussed the corresponding parameters of the proposed transfer function in detail. Finally, both the *in vivo* measurement and the corresponding simulation of the galvanic coupling IBC were carried out along the different transmission paths. Moreover, the corresponding simulation results and the measurement results were also analyzed.

The rest of this paper is organized as follows. Section II describes the circuit model and the transfer function of the galvanic coupling IBC. Section III focuses on the determination of the corresponding parameters used in the proposed transfer function. The mathematical simulations based on the proposed transfer function and the *in vivo* measurements are presented in Section IV. Section V concludes this paper.

II. TRANSFER FUNCTION

A. Circuit Model

The establishment of the circuit model is the first step to achieve the transfer function of the galvanic coupling IBC. In the galvanic coupling IBC, the signal is transmitted from the transmitter to the receiver by coupling a signal into the human body, as shown in Fig. 2.

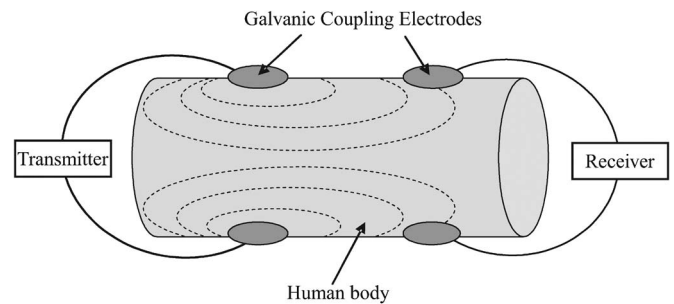


Fig. 2. Schematic diagram of the galvanic coupling IBC.

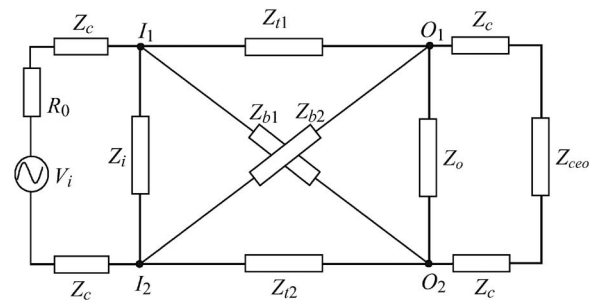


Fig. 3. Four-terminal circuit model of the galvanic coupling IBC.

According to Fig. 2, the signal transmission of the galvanic coupling IBC can be described by the four-terminal circuit model shown in Fig. 3 in which all the impedances of the connecting wires were ignored. In Fig. 3, Z_c represents the coupling impedance between the transmitting electrode and the skin, while the two transmitting electrodes are attached to the human skin at I_1 and I_2 , respectively. Additionally, the impedance of Z_i , which represents the impedance between I_1 and I_2 , is treated as the input impedance of the human body. On the other hand, Z_{t1} and Z_{t2} are the transverse impedances of the transmission path, while Z_{b1} and Z_{b2} are the cross impedances of the transmission path in the human body. Similarly, the output impedance of the human body is represented as Z_o , while the coupling impedance between the receiving electrode and the skin is also represented as Z_c . It should be noted that the internal impedances of the IBC devices also influence the signal transmission characteristic of the galvanic coupling IBC. For instance, the use of the electrooptic crystal sensor with a high input impedance has greatly increased the data transmission rate (up to 10 Mb/s) [2], [11]. Therefore, both the output resistor

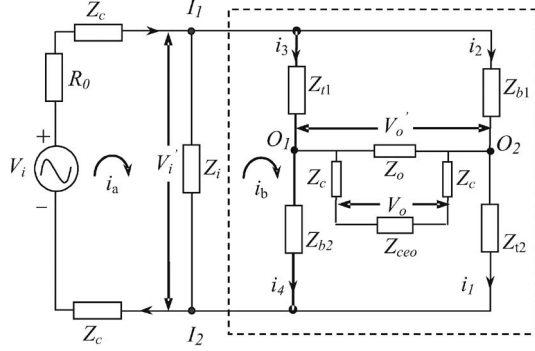


Fig. 4. Equivalent circuit of the galvanic coupling IBC.

of the transmitter (R_o) and the input impedance of the receiver (Z_{ceo}) are included in our circuit model.

B. Derivation of the Transfer Function

Based on the proposed circuit model, the transfer function of the galvanic coupling IBC can be derived. The equivalent circuit of Fig. 3 is shown in Fig. 4 in which V_i is the output voltage of the transmitter, while V_i' is the voltage between I_1 and I_2 . Similarly, V_o represents the input voltage of the receiver, while V_o' represents the voltage between O_1 and O_2 . As a result, the following equation can then be obtained.

$$\begin{cases} i_2 + i_3 = i_1 + i_4 \\ V_o' = i_2 Z_{b1} - i_3 Z_{t1} = i_4 Z_{b2} - i_1 Z_{t2} \\ V_i' = i_2 Z_{b1} + i_1 Z_{t2} \end{cases} \quad (1)$$

On the other hand, the impedance between O_1 and O_2 can be represented as Z_o' , and

$$Z_o' = \frac{Z_o(2Z_c + Z_{ceo})}{Z_o + 2Z_c + Z_{ceo}}. \quad (2)$$

As a result, the transfer function of the circuit between I_1 and I_2 can be calculated according to (1), leading to the following equation:

$$H_h = \frac{V_o'}{V_i'} = \frac{(i_1 - i_2)Z_o'}{i_2 Z_{b1} + i_1 Z_{t2}} = \frac{(k-1)Z_o'}{Z_{b1} + kZ_{t2}} \quad (3)$$

where H_h denotes the transfer function of the circuit between I_1 and I_2 and k is expressed as

$$k = \frac{i_1}{i_2} = \frac{Z_{b2}Z_{t1} + Z_{b2}Z_o' + Z_{b1}Z_{b2} + Z_o'Z_{t1}}{Z_{b2}Z_{t1} + Z_{b2}Z_o' + Z_{t1}Z_{t2} + Z_o'Z_{t1}}. \quad (4)$$

In the following discussion, the Z_c of the transmitting terminal is introduced. First, the circuit of the dotted portion shown in Fig. 4 is simplified as the impedance of Z_h , resulting in the following equation:

$$\frac{V_i'}{V_i} = \frac{Z_i Z_h}{Z_i Z_h + (2Z_c + R_o)(Z_i + Z_h)} \quad (5)$$

where $Z_h = V_i'/(i_2 + i_3)$. On the other hand, according to (1), i_3 can be expressed as

$$i_3 = \frac{i_2 Z_{b1} - (i_1 - i_2)Z_o'}{Z_{t1}} = \frac{i_2(Z_{b1} + Z_o') - i_1 Z_o'}{Z_{t1}}. \quad (6)$$

According to (5) and (6), the following equation can be obtained.

$$\frac{1}{Z_h} = \frac{i_2 + i_3}{V_i'} = \frac{i_2(Z_{t1} + Z_{b1} + Z_o') - i_1 Z_o'}{Z_{t1} V_i'}. \quad (7)$$

On the other hand, according to (1), the currents of i_1 and i_2 can be expressed as

$$i_1 = \frac{Z_o V_i' + Z_{b1} V_o'}{Z_o Z_{t2} + Z_o Z_{b1}}, \quad i_2 = \frac{Z_o V_i' - Z_{t2} V_o'}{Z_o Z_{t2} + Z_o Z_{b1}}. \quad (8)$$

Substitute i_1 and i_2 into (7), leading to the following equation:

$$\frac{1}{Z_h} = \frac{(Z_{t1} + Z_{b1} + Z_o' - kZ_o')(Z_o' - Z_{t2}H_h)}{Z_{t1}(Z_{t2}Z_o' + Z_{b1}Z_o')} \quad (9)$$

where $H_h = V_o'/V_i'$. Therefore, the transfer function of H_h' , which represents the transfer function of the human body, the transmitting electrodes, and the transmitter itself, can be expressed as

$$H_h' = H_h \frac{V_i'}{V_i} = \frac{Z_i Z_h H_h}{Z_i Z_h + (2Z_c + R_o)(Z_i + Z_h)}. \quad (10)$$

Based on the aforementioned discussion, the whole transfer function of the galvanic coupling IBC (H_A) can be expressed as the following equation.

$$H_A = \frac{V_o}{V_i} = \frac{V_o' V_o}{V_i V_o'} = H_h' \frac{Z_{ceo}}{Z_{ceo} + 2Z_c}. \quad (11)$$

Substituting H_h' back to (11) yields

$$H_A = \frac{Z_i Z_h}{Z_i Z_h + (2Z_c + R_o)(Z_i + Z_h)} \cdot \frac{Z_{ceo}}{Z_{ceo} + 2Z_c} H_h. \quad (12)$$

As a result, the whole transfer function of the galvanic coupling IBC can be expressed as (12) and the corresponding equations in (2)–(4) and (9). Finally, the attenuation of the signal transmission in the galvanic coupling IBC can be determined by

$$A = 20 \log_{10} H_A + K \quad (13)$$

where K is the correction factor used for correcting the inherent error between the measurements and the simulations. Generally, K is influenced by the modeling method, the parameter determination, the measurement precision, etc.

III. PARAMETERS

To achieve the mathematical simulation of the IBC, the corresponding parameters of the transfer function method should be determined correctly. The following is the discussion of the parameters used in the proposed transfer function.

A. Modeling of the Human Body

First, to determine the parameters of the proposed transfer function, the human body was transformed into a model identified as the head, arm, torso, and leg. The body parts have complex geometry and internal structure. However, according to the previous research results of IBC, a more detailed geometry

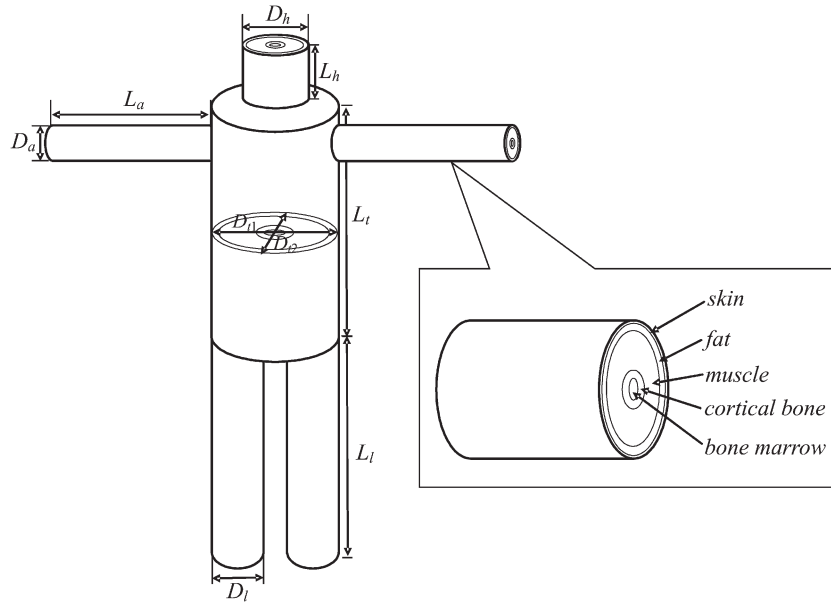


Fig. 5. Modeling of the human body.

with complex layer structures would not significantly improve the results [6]. Therefore, to simplify the IBC model and the parameter determination, all the human parts were abstracted as the concentric cylinders or the concentric elliptical cylinder consisting of the layers of the skin, fat, muscle, cortical bone, and bone marrow in our investigation, as shown in Fig. 5.

In our investigation, the geometry of the head is modeled by the cylinder with the diameter D_h and the height L_h . Similarly, the geometry of the arms is modeled by two cylinders with the diameter D_a and the height L_a . The geometry of the torso was modeled by an elliptic cylinder, which has the long-axis diameter D_{t1} , the short-axis diameter D_{t2} , and the height L_t . Moreover, the legs are approximated by two cylinders with the diameter D_l and the height L_l . According to [14], the thicknesses of the different layers in a human arm with a radius of 50 mm are 1.5 (skin), 8.5 (fat), 27.5 (muscle), 6 (cortical bone), and 6.5 mm (radius, bone marrow layers). To simplify the simulation process, the thicknesses of the corresponding layers in the human body model shown in Fig. 5 were set in proportion to the thicknesses previously mentioned. As for the different types of the human body, it has different geometry parameters corresponding to our models. As shown in Fig. 5, different persons may have the different lengths, radius, and heights corresponding to the cylinders or the elliptic cylinder, may also have the different thicknesses of the different tissue layers, etc. The differences of these parameters will result in the different impedances of the signal transmission path. Finally, it will result in the different results in the galvanic coupling IBC simulation.

On the other hand, the dielectric properties of the human tissues can be expressed as the conductivity and the relative permittivity. The conductivity and the relative permittivity of the human body have been investigated by Gabriely *et al.*, and some of their results are shown in Table I [15], where σ is the conductivity and ϵ_r represents the relative permittivity. These two parameters, which vary with the different tissue layers and signal frequencies, are suitable for the different human bodies.

TABLE I
CONDUCTIVITIES AND THE RELATIVE PERMITTIVITIES

	Freq. (kHz)	Skin (wet)	Fat	Muscle	Cortical bone	Bone marrow
σ	100	4.0E-2	2.8E-2	3.9E-1	2.0E-2	8.5E-2
	200	9.0E-2	3.5E-2	4.4E-1	2.2E-2	8.7E-2
	500	1.3E-1	4.5E-2	5.0E-1	2.5E-2	9.0E-2
	700	1.6E-1	4.5E-2	5.6E-1	2.5E-2	9.5E-2
	1000	2.0E-1	4.5E-2	6.0E-1	2.5E-2	1.0E-1
	1500	2.3E-1	4.5E-2	6.2E-1	2.7E-2	1.0E-1
	2000	2.5E-1	4.6E-2	6.3E-1	2.8E-2	1.1E-1
ϵ_r	5000	3.5E-1	4.7E-2	6.8E-1	4.0E-2	1.2E-1
	100	2.0E+4	1.0E+2	8.0E+3	2.5E+2	5.0E+2
	200	1.4E+4	6.5E+1	6.3E+3	2.1E+2	4.0E+2
	500	8.0E+3	4.0E+1	4.0E+3	2.0E+2	3.5E+2
	700	4.5E+3	3.3E+1	3.5E+3	1.8E+2	2.7E+2
	1000	3.5E+3	3.0E+1	3.0E+3	1.6E+2	2.5E+2
	1500	2.1E+3	2.7E+1	2.5E+3	1.4E+2	2.2E+2
2000	1.5E+3	2.6E+1	2.2E+3	1.3E+2	1.9E+2	
5000	5.0E+2	2.0E+1	4.0E+2	6.0E+1	1.3E+2	

B. Impedances of Z_t

The values of the transverse impedance (Z_t) shown in Fig. 3 are mainly affected by the length of the signal transmission path, the dielectric properties of the human tissues, and the geometric parameters of the human body. Based on the modeling of the human body shown in Fig. 5, the values of Z_t can be determined according to the geometries of the particular human parts and the results in Table I.

First, we assume that m represents a particular part of the human body model, such as the head, arm, torso, or leg, while Z_{mt} represents the transverse impedance within the m part of the human body. Due to the human part which consists of

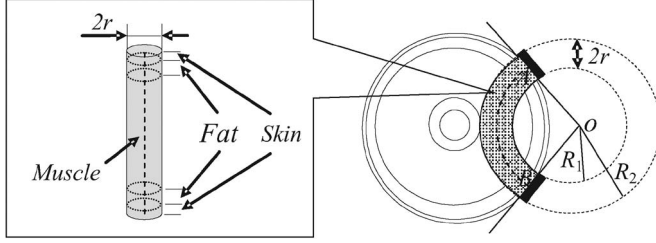


Fig. 6. Determination of Z_i and Z_o .

five layers (skin, fat, muscle, cortical bone, and bone marrow), then Z_{mt} can be expressed as the parallel connection of the impedances corresponding to the different layers

$$\begin{aligned} Z_{mt} &= \frac{1}{\sum_{l=1}^5 \frac{1}{Z_{ml}}} = \frac{1}{\sum_{l=1}^5 \left(\frac{1}{R_{ml}} + j\omega C_{ml} \right)} \\ &= \frac{L_m}{\sum_{l=1}^5 \sigma_{lf} S_{ml} + j\omega \epsilon_0 \sum_{l=1}^5 \epsilon_{rlf} S_{ml}} \end{aligned} \quad (14)$$

where L_m is the length of the signal transmission path. S_{ml} is the cross-sectional area of the l th layer. σ_{lf} and ϵ_{lf} are the conductivity and the relative permittivity corresponding to the different layers and signal frequencies, respectively.

In the galvanic coupling IBC with different signal transmission paths, the signal transmits within different human parts. In this case, the transverse impedance of Z_t can be determined by summing all the Z_{mt} 's within the path.

C. Impedances of Z_i and Z_o

Due to the requirement of high accuracy of the measurement device and the instability of the measurement conditions, generally, it is difficult to measure the input impedance (Z_i) and the output impedance (Z_o) of the human body accurately. In this paper, a new method is proposed to determine the values of Z_i and Z_o .

According to the previous simulation results [6], the relatively high current corresponding to Z_i or Z_o mainly focuses on the sector ring section between the two transmitting electrodes or the receiving electrodes. In our investigation, the sections can be described as an intersection between a ring and the cylinder model. First, we assumed that two circular electrodes with a radius r are attached to the cylinder model, A and B are the tangent points between the electrodes and the surface of the cylinder model, and OA and OB are the two tangents which intersect at O , as shown in Fig. 6. Then, set O as a circular center; a ring with the inner radius $R_1 = OA - r$ and the outer radius $R_2 = OA + r$ can be formed. The intersection between the ring and the cylinder model, which was represented as the shadow part in Fig. 6, was used for determining the values of Z_i and Z_o . In our investigation, the intersection is considered as a cylinder called the input or output impedance (IOI) cylinder, as shown in Fig. 6. The height of the IOI cylinder is equal to the axis length of the shadow part, while its diameter is equal to $2r$. In general, the IOI cylinder consists of two skin layers, two fat layers, and one muscle layer. According to the difference of

the geometric relationship between the ring and the particular cylinder, the cortical bone layer and the bone layer may also be included in the IOI cylinder.

Finally, according to the geometry of the IOI cylinder and the values shown in Table I, the values of Z_i and Z_o can be determined by using the following equation:

$$\begin{aligned} Z_i = Z_o &= \sum_{l=1}^5 \frac{1}{\frac{1}{R_l} + j\omega C_l} = \sum_{l=1}^5 \frac{1}{\frac{\sigma_{lf} S}{L_l} + j\omega \frac{\epsilon_{rlf} \epsilon_0 S}{L_l}} \\ &= \sum_{l=1}^5 \frac{L_l}{\sigma_{lf} \pi r^2 + j\omega \epsilon_{rlf} \epsilon_0 \pi r^2} \end{aligned} \quad (15)$$

where L_l represents the thickness of the different layers (skin, fat, muscle, etc.).

D. Impedances of Z_b and Z_c

In the circuit model of the galvanic coupling IBC shown in Fig. 3, Z_{b1} is the cross impedance between I_1 and O_2 , while $Z_t = Z_{t1} = Z_{t2}$. If the Z_{b1} is divided into the transverse component and the longitudinal component, then the transverse component of Z_{b1} is equal to Z_{t1} representing the impedance between I_1 and O_1 , while the longitudinal component of Z_{b1} is equal to Z_o representing the impedance between O_1 and O_2 . As a result, the value of Z_{b1} can be set as the sum of Z_t and Z_o . Similarly, the value of Z_{b2} can also be set as the sum of Z_t and Z_i .

On the other hand, in the galvanic coupling IBC, the value of Z_c shown in Fig. 3 is mainly influenced by the electrode size, the impedance of the human skin, and the distance between the electrode and the skin. Since the theoretical method used for determining the value of Z_c remains unsolved, the values of Z_c used in our simulations were determined according to the measurement results of Wegmueller *et al.* [8].

IV. SIMULATIONS AND MEASUREMENTS

A. Method

To verify the feasibility of the proposed transfer function, both the *in vivo* measurements of the galvanic coupling IBC and the corresponding mathematical simulation based on the proposed transfer function were carried out along the different signal transmission paths. The measurement setup, as shown in Fig. 7, was composed of a signal generator, a digital oscilloscope, and the galvanic coupling electrodes in which the signal generator (SG1040, $R_o = 50 \Omega$, made by Jiangsu Right Electronic Equipment Company, Ltd., China) was used for providing the signal output at the transmitting terminal, the digital oscilloscope (Agilent 54641A, $R_{ceo} = 1 \text{ M}\Omega$ and $C_{ceo} = 13 \text{ pF}$) was used for the signal measurement at the receiving terminal, and the galvanic coupling electrodes, including two pairs of circular copper electrodes, were used for coupling the signal into the human body and receiving the signal transmitted within the human body. Each electrode has the radius of 10 mm.

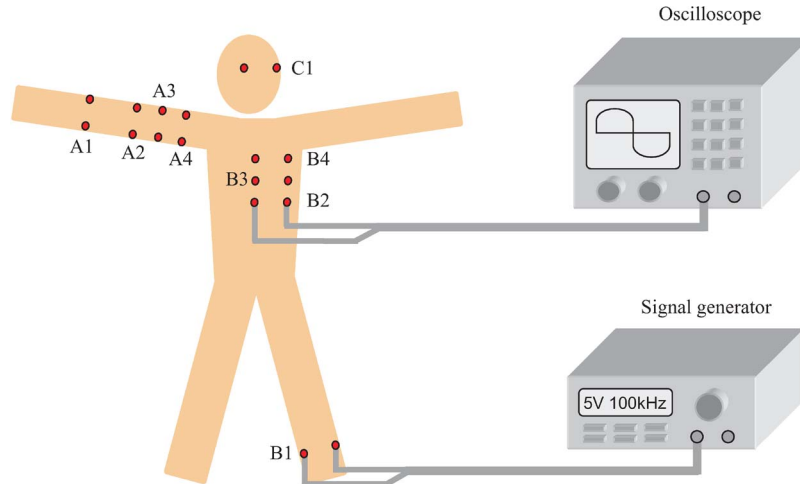


Fig. 7. Measurement setup.

TABLE II
PHYSIOLOGICAL PARAMETERS AND THE GEOMETRIES OF THE SUBJECTS

Subject	Age	BMI	Weight	Height	Head	Arm	Leg	Torso	
					D_h	D_a	D_l	D_{t1}	D_{t2}
Male	24	22.3	70kg	177cm	18cm	9cm	16cm	28cm	19cm
Female	23	18.3	48kg	162cm	17cm	7.5cm	14cm	25cm	15cm

Unless otherwise indicated, the two pairs of electrodes at the transmitting terminal and the receiving terminal were both attached with 8-cm spacing.

On the other hand, two people were chosen as the subjects; one is male and has a normal weight, while the other is female and underweight. Table II shows the physiological parameters and the geometries of the subjects.

In our measurement, the sine wave signals with the amplitude of 5 V (peak-to-peak value) were applied on the transmitting electrodes. The considerations of the signal frequency used in our experiments include the following: 1) The existing research shows that the power spectrum of the electrical signals produced by the biological processes mainly covers the low-frequency range [14], and therefore, the IBC system should avoid using the low-frequency signals, and 2) there is also the limitation of the circuit model in the high-frequency range. Finally, the frequency range from 100 kHz to 5 MHz was chosen as the signal frequency used in our measurements and simulations. In our *in vivo* measurements, the signal attenuations of the galvanic coupling IBC were calculated according to the following equation:

$$\text{Attenuation} = 20 \log_{10} \left(\frac{U_{\text{receiver}}}{U_{\text{transmitter}}} \right) \quad (16)$$

where $U_{\text{transmitter}}$ represents the voltage at the transmitting electrodes, while U_{receiver} represents the voltage at the receiving electrodes. Additionally, all the measurements corresponding to the different detection points and signal frequencies were repeated and recorded for three times, while the average values of the three results were chosen as the measured values.

B. Signal Transmission Along the Arm

First, the *in vivo* measurements of the signal attenuation in the galvanic coupling IBC were carried out along the arms of the subjects. As shown in Fig. 7, the transmitting electrodes were placed on the positions of A_1 , while the receiving electrodes were placed on A_2 , A_3 , and A_4 , resulting in the signal transmission distance of 20, 30, and 40 cm, respectively. In the measurements with the female subject, the two pairs of electrodes at the transmitting terminal and the receiving terminal were both attached with 6-cm spacing. Meanwhile, the corresponding simulations based on the proposed transfer function were carried out according to the geometries of the subjects.

1) *Determination of K* : Due to the influence of the modeling method, the parameter determination, the measurement precision, etc., the difference between the simulation results and the measurement results is inevitable. In our investigation, the K in (13) is determined by the inherent error between the measurement results and the simulation results. According to the comparison between the measurement results and the simulation results, it can be found that there is an approximately constant error between the two results corresponding to a particular signal transmission path. As a result, the constant error can be set as the value of K . For instance, in Fig. 8(a), which shows the signal attenuations of the measurement and simulation results of the male subject, it can be found that there is an approximately fixed error between the two results corresponding to the three signal transmission distances (20, 30, and 40 cm), while the average value of the fixed error is 19.88 dB. Moreover, the similar phenomenon can also be found in Fig. 8(b), which shows the errors between the measurement

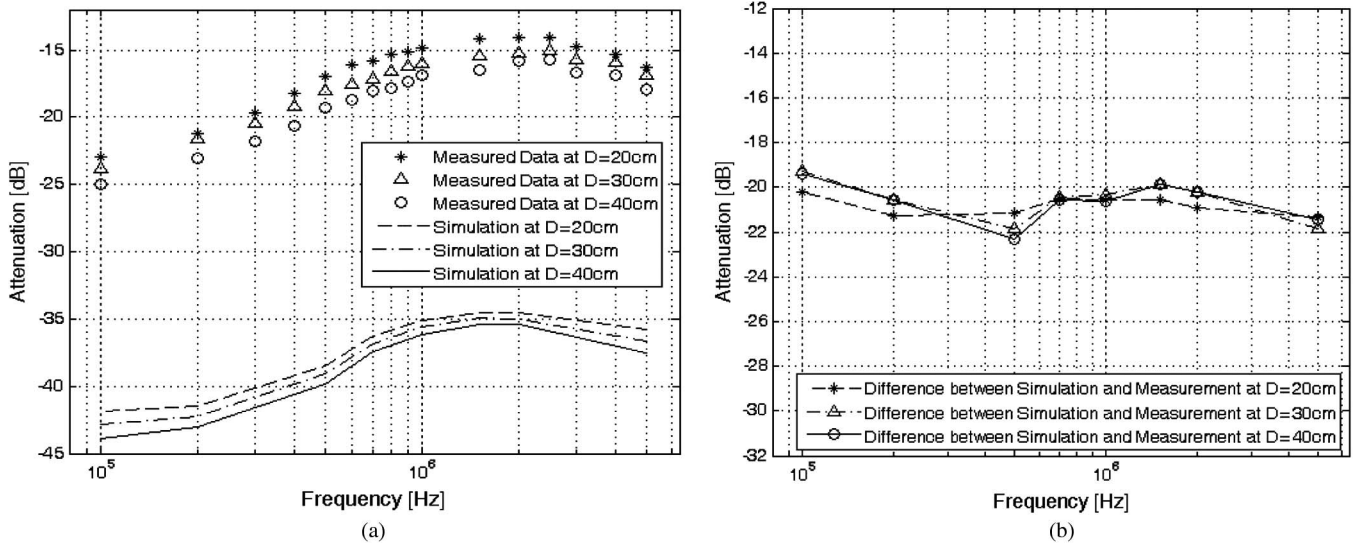


Fig. 8. Simulation results and the measurement results of the arm path. (a) Results of the male subject. (b) Simulation errors of the female subject.

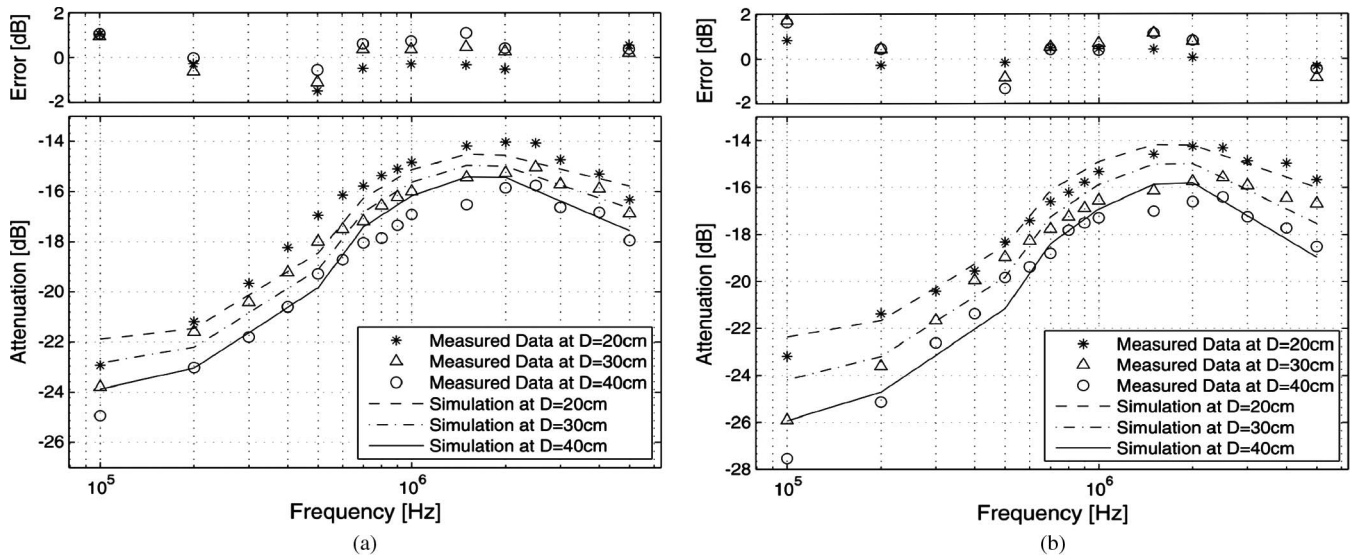


Fig. 9. Measurement results and the simulation results corrected by the K of the arm path. (a) Results of the male subject. (b) Simulation errors of the female subject.

and the simulation of the female subject. The standard deviation of the errors shown in Fig. 8(b) is 0.75 dB, while the average value is 20.67 dB. Therefore, the values of K corresponding to the arm path were finally set as 19.88 (the male subject) and 20.67 dB (the female subject).

According to the results previously mentioned, we also can find that the K value of the male subject (19.88 dB) is close to the value of the female subject (20.67 dB). Generally, in the case of IBC simulation with low precision, the value of K corresponding to the arm path can also be set as the average value of the two K values (20.28 dB). On the other hand, in the case of IBC simulation with high precision, due to the error between the simulation and the measurement which is influenced by the matching degree between the model and the actual human body, K changes along with the different signal transmission paths and the different human bodies. Therefore, in order to achieve the high simulation precision, the *in vivo*

measurement corresponding to the particular signal transmission path within the actual human body should be carried out at one or more specific signal frequencies; then, the value of the K corresponding to the particular signal transmission path of the human body can be determined by comparing the measurement results and the simulation results.

2) *Comparison Between the Simulation and the Measurement:* The measurement results and the simulation results corrected by K of the arm path are shown in Fig. 9, which also includes the errors corresponding to each signal frequency and transmission distance. It can be seen from Fig. 9 that the mathematical simulation results based on the proposed transfer function basically agree with the corresponding measurement results. Both the simulation results and the *in vivo* measurement results are decreased as the signal frequency increased from 100 kHz to 2 MHz and increased gradually as the signal frequency increased from 2 to 5 MHz. Meanwhile, the absolute

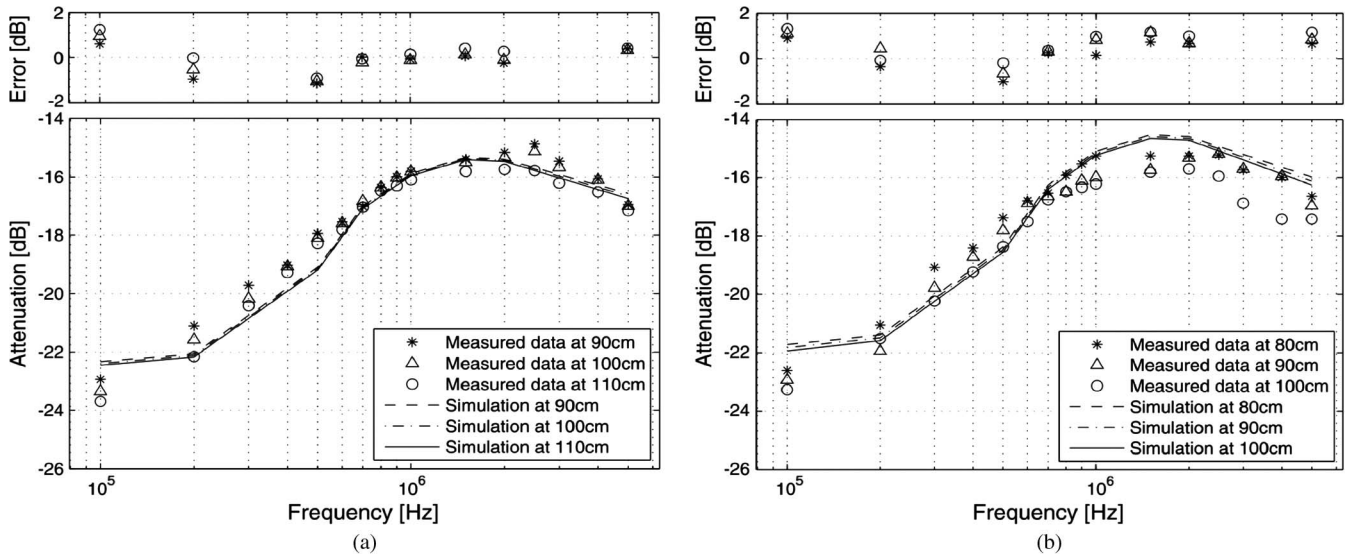


Fig. 10. Simulation results and the measurement results of the path from the leg to the torso. (a) Results of the male subject. (b) Simulation errors of the female subject.

values of the errors between the simulation and the measurement are limited to 2 dB. On the other hand, when the transmission distance is increased from 20 to 40 cm, the corresponding increase of the signal attenuations can also be found in the two results. For instance, according to Fig. 9(b), an increase of 10 cm of the signal transmission distance leads to an extra average attenuation of 1.24 dB in the simulation results, while the corresponding value in the measurement results is 1.19 dB, indicating that both of the two transfer functions are sensitive to the signal transmission distance in this path. Moreover, it can also be noted that the extra average attenuations caused by the increase of the signal transmission distance are relatively bigger. The main reason resulting in this phenomenon is that the diameter of the female subject's arm (7.5 cm) is less than that of the male subject's arm (9 cm).

C. Signal Transmission Within the Different Human Parts

In these experiments, two kinds of applications are considered: 1) Signal is transmitted from the IBC shoe to the electronic devices (such as personal digital assistant (PDA), MP4, cell phone, etc.) attached to the torso, resulting in the path between the foot and the torso, and 2) signal is transmitted from the IBC shoe to the earphone, resulting in the signal transmission path from the foot to the ear. To simplify the simulation process, the foot itself was not included in the paths of the measurements and simulations.

1) *Transmission Path From the Leg to the Torso*: The signal transmission path from the leg to the torso includes the whole leg and some parts of the torso. First, the IBC transmitting electrodes were placed on the ankle of the subjects (B_1); then, the receiving electrodes were placed on the positions of B_2 , B_3 , and B_4 , as shown in Fig. 7. In this measurement, the signal transmission distances of the male subject were set as 90, 100, and 110 cm, respectively. Due to the limitation of the female's height (162 cm), the signal transmission distances within her body were set as 80, 90, and 100 cm, respectively. Meanwhile,

the corresponding simulations based on the proposed transfer function were carried out. Both the signal attenuations of the measurement and that of the simulation are shown in Fig. 10 in which K was set as 19.02 (male) and 19.48 dB (female).

From Fig. 10, it can be observed that the mathematical simulation results of the leg–torso path also agree with the corresponding measurement results. Moreover, the average value of the errors between the simulation results and the measurement results of the male subject is 0.43 dB, while that of the female subject is 0.71 dB, indicating that the simulation results based on the proposed transfer function coincide with the corresponding measurement results in these experiments. Furthermore, we also can find from Figs. 9 and 10 that, even the signal transmission distance of this path is longer than that of the arm path, the signal attenuations of the leg–torso path are less than that of the arm path. Moreover, the increment of the signal attenuations corresponding to the increase of the transmission distance (10 cm) shown in Fig. 10 is comparatively less than that of the signal attenuations shown in Fig. 9. This phenomenon can be explained by the fact that the cross-sectional areas of the torso and leg are bigger than that of the arm. As for the male subject, the diameter of the arm is only 9 cm, while the diameter of the leg is 16 cm, and the geometry parameters of the torso are $D_{t1} = 28$ cm and $D_{t2} = 19$ cm. As a result, the impedances of the arm path are much larger than that of the path from the leg to the torso. For instance, when the signal frequency is 100 kHz, the R_t of the arm path (40 cm) is 263.8 Ω , while the R_t of the leg–torso path (90 cm) is only 166.1 Ω . Therefore, the signal attenuation of the arm path is bigger than that of the leg–torso path. Meanwhile, the increase of the signal transmission distance of the leg–torso path results in the comparatively smaller attenuations.

2) *Transmission Path From the Leg to the Ear*: In the *in vivo* measurement of the path from the leg to the ear, the transmitting electrodes were also placed on B_1 , and the receiving electrodes were placed on the position below the subjects' ear (C_1), as shown in Fig. 7. This path, including the leg, torso, and head,

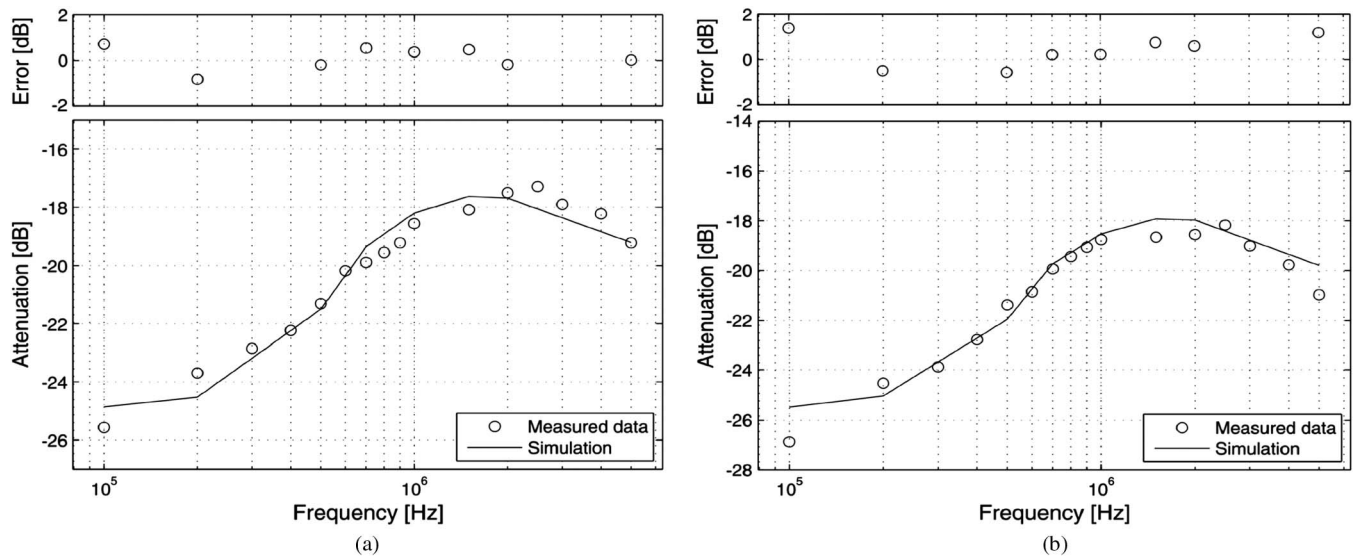


Fig. 11. Simulation results and the measurement results of the path from the foot to the ear. (a) Results of the male subject. (b) Simulation errors of the female subject.

has the signal transmission distance of 145 (the male subject) and 130 cm (the female subject). Both the measurement results and the corresponding simulation results of this path are shown in Fig. 11 in which K was set as 16.89 (male) and 16.59 dB (female).

It can be seen from Fig. 11 that the signal attenuation curves of the simulation results have a similar outline with the measurement results over the signal frequency from 100 kHz to 5 MHz, while the average errors between the simulation results and the measurement results are 0.41 (the male subject) and 0.68 dB (the female subject). In addition, it should be noted that the increments of the signal attenuation corresponding to the transmission distance of the simulation results are close to that of the measurement results in these experiments. For instance, according to the results of the female subject, the average increments of the simulation results and that of the measurement results are 3.56 and 3.75 dB, respectively, when the transmission distances are increased from 80 to 130 cm, as shown in Fig. 11(b), which indicates that the proposed model has the similar sensitivity corresponding the actual leg–ear path.

D. Discussion of the Results

According to the results previously mentioned, some discussions are therefore deduced as follows: 1) By using the proposed human body model with five layers and the circuit model with the impedances of the IBC devices, the simulation of the galvanic coupling IBC can be achieved with comparatively high precision; 2) due to the geometry of the whole human body model that is corresponding to that of the actual human body, the IBC simulation with the different signal transmission paths within the different human bodies can be achieved; and 3) the frequency characteristics of the galvanic coupling IBC can be achieved by using the proposed human body model corresponding to the signal frequency. Meanwhile, according to the simulation results, the relatively small attenuations are generally located in the frequency range of 1–2 MHz. Therefore, to

reduce the power consumption of the IBC devices, it is better to set the carrier frequency of the IBC system in this range.

V. CONCLUSION

In this paper, a simulation method of the galvanic coupling IBC with different signal transmission paths has been proposed by deriving the transfer function and discussing the corresponding parameters. To verify the validity of the proposed transfer function, both the *in vivo* measurements and the corresponding mathematical simulations based on the proposed transfer function were carried out along the different signal transmission paths. Finally, the close agreement between the simulation results and measurement results has been demonstrated, which indicates that the proposed transfer function will offer significant advantages in the theoretical analysis and the application of the galvanic coupling IBC.

The advantages of the proposed methods can be described as follows: 1) It has the comparatively high precision in the simulation of the galvanic coupling IBC; 2) the IBC simulation with different signal transmission paths can be achieved by using the proposed method and model; and 3) based on the proposed method and model, the frequency characteristics of the galvanic coupling IBC can be achieved. On the other hand, compared with the simple models, the computational cost of the IBC simulation based on the proposed method is relatively bigger.

Recently, the proposed model and method have been suitable for the simulation of the signal transmission among the electronic devices attached on the human skin. Our next work will focus on the simulation of implanting IBC.

ACKNOWLEDGMENT

The authors would like to thank the Institute of Optics and the Writing Center of the University of Rochester, Rochester, NY, for their help.

REFERENCES

- [1] T. G. Zimmerman, "Personal area networks (PAN): Near-field intra-body communication, in media art and science," M.S. thesis, MIT, Cambridge, U.K., 1995.
- [2] M. Shinagawa, M. Fukumoto, K. Ochiai, and H. Kyuragi, "A near-field-sensing transceiver for intrabody communication based on the electrooptic effect," *IEEE Trans. Instrum. Meas.*, vol. 53, no. 6, pp. 1533–1538, Dec. 2004.
- [3] M. S. Wegmueller, S. Huclova, J. Froehlich, M. Oberle, N. Felber, N. Kuster, and W. Fichtner, "Galvanic coupling enabling wireless implant communications," *IEEE Trans. Instrum. Meas.*, vol. 58, no. 8, pp. 2618–2625, Aug. 2009.
- [4] M. S. Wegmueller, M. Oberle, N. Felber, N. Kuster, and W. Fichtner, "Signal transmission by galvanic coupling through the human body," *IEEE Trans. Instrum. Meas.*, vol. 59, no. 4, pp. 963–969, Aug. 2010.
- [5] T. Handa, "A very low-power consumption wireless ECG monitoring system using body as a signal transmission medium," in *Proc. Int. Conf. Solid-State Sens. Actuators*, 1997, pp. 1003–1006.
- [6] M. S. Wegmueller, A. Kuhn, J. Froehlich, M. Oberle, N. Felber, N. Kuster, and W. Fichtner, "An attempt to model the human body as a communication channel," *IEEE Trans. Biomed. Eng.*, vol. 54, no. 10, pp. 1851–1857, Oct. 2007.
- [7] Y. Song, G. Yang, Q. Hao, and M. Wang, "The simulation of electrostatic coupling intra-body communication based on finite-element models," *Proc. SPIE*, vol. 7157, pp. 71570D1–71570D8, 2009.
- [8] M. S. Wegmueller, M. Oberle, N. Felber, N. Kuster, and W. Fichtner, "Galvanical coupling for data transmission through the human body," in *Proc. IMTC*, Sorrento, Italy, Apr. 2006, pp. 1686–1689.
- [9] N. Cho, J. Yoo, S.-J. Song, J. Lee, S. Jeon, and H.-J. Yoo, "The human body characteristics as a signal transmission medium for intrabody communication," *IEEE Trans. Microw. Theory Tech.*, vol. 55, no. 5, pp. 1080–1085, May 2007.
- [10] K. Hachisuka, A. Nakata, T. Takeda, K. Shiba, K. Sasaki, H. Hosaka, and K. Itao, "Development of wearable intra-body communication devices," *Sens. Actuators A, Phys.*, vol. 105, no. 1, pp. 109–115, Jun. 2003.
- [11] A.-I. Sasaki, M. Shinagawa, and K. Ochiai, "Principles and demonstration of intrabody communication with a sensitive electrooptic sensor," *IEEE Trans. Instrum. Meas.*, vol. 58, no. 2, pp. 457–466, Dec. 2009.
- [12] K. Hachisuka, Y. Terauchi, Y. Kishi, K. Sasaki, T. Hirota, H. Hosaka, K. Fujii, M. Takahashi, and K. Ito, "Simplified circuit modeling and fabrication of intra body communication devices," *Sens. Actuators A, Phys.*, vol. 130/131, pp. 322–330, Aug. 2006.
- [13] R. Xu, H. Zhu, and J. Yuan, "Circuit-coupled FEM analysis of the electrical-field type intra-body communication channel," in *Proc. IEEE BioCAS*, 2009, pp. 221–224.
- [14] M. S. Wegmueller, "Intra-body communication for biomedical sensor networks," Ph.D. dissertation, ETH Zurich, Zurich, Switzerland, 2007.
- [15] S. Gabriely, R. W. Lau, and C. Gabriel, "The dielectric properties of biological tissues: III. Parametric models for the dielectric spectrum of tissues," *Phys. Med. Biol.*, vol. 41, no. 11, pp. 2271–2293, Nov. 1996.



Yong Song received the Ph.D. degree from the Beijing Institute of Technology, Beijing, China, in 2004.

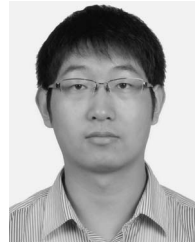
Since 2004, he has been an Assistant Professor with the School of Optoelectronics, Beijing Institute of Technology. In 2007, he was an Associate Professor with the School of Information Science and Technology, Beijing Institute of Technology. From October 2009 to April 2010, he was a Visiting Scientist with the Institute of Optics, University of Rochester, Rochester, NY. His research interests include intrabody communication, optoelectronic detection, and wireless multi-

media sensor networks.



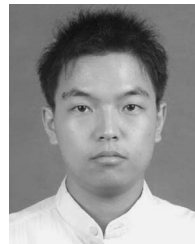
Qun Hao received the Ph.D. degree from Tsinghua University, Beijing, China, in 1997.

In 1999, she was a Visiting Scholar with the University of Tokyo, Tokyo, Japan. Since 2003, she has been a Professor with the School of Optoelectronics, Beijing Institute of Technology, Beijing. Her research interests include optics and precision measurement and optoelectronic sensor technology.



Kai Zhang received the B.E. degree from the School of Optoelectronics, Beijing Institute of Technology, Beijing, China, in 2008. He is currently working toward the Ph.D. degree in the Modern Optoelectronics Instrument Laboratory, School of Optoelectronics, Beijing Institute of Technology.

His research interests include intrabody communication, the modeling and simulation of optoelectronic systems, and optoelectronic sensor technology.



Ming Wang received the B.E. degree from the School of Information Science and Engineering, Shandong University, Jinan, China, in 2002. He is currently working toward the Ph.D. degree in the Modern Optoelectronics Instrument Laboratory, School of Optoelectronics, Beijing Institute of Technology, Beijing, China.

His research interests include the modeling and simulation of optoelectronic systems, optical manufacturing, and testing technologies.



Yifang Chu received the B.E. degree from the School of Optoelectronic Engineering, Xi'an Technological University, Xi'an, China, in 2008. She is currently working toward the M.E. degree in the Modern Optoelectronics Instrument Laboratory, School of Optoelectronics, Beijing Institute of Technology, Beijing, China.

Her research interests include finite-element method simulation and intrabody communication.



Bangzhi Kang received the B.E. degree from the School of Optoelectronics, Beijing Institute of Technology, Beijing, China, in 2008. He is currently working toward the M.E. degree in the Modern Optoelectronics Instrument Laboratory, School of Optoelectronics, Beijing Institute of Technology.

His research interests include circuit design and intrabody communication.